CrossMark

CPPTA3

Photopyroelectric Characterization of Magnetic Nanofluids. Influence of Type and Size of Nanoparticles on the Thermal Parameters

D. Dadarlat[1] · **I. Craciunescu**[1] · **R. Turcu**[1] ·
C. Tripon[1]

Abstract The influence of type and size of nanoparticles on the thermal parameters of some magnetic nanofluids is investigated. Two types of carrier liquids (transformer oil and polypropylene glycol) were combined with two types of iron based magnetic nanoparticles (Fe_3O_4 and $MnFe_2O_4$). Different sizes (10 nm–80 nm) and shapes (spherical, octahedral or cubic) of nanoparticles were obtained depending on the oleic acid/oleylamine molar ratio, which drastically influences the nanocrystals growth rate. This influence is due to the different binding ability of the two stabilizers onto crystal facets. The average size of nanoparticles was 10 nm, 35 nm and 50 nm for Fe_3O_4 and 10 nm, 20 nm and 80 nm for $MnFe_2O_4$ at a concentration of $50\,mg\cdot ml^{-1}$ in all cases. The results obtained by PPE technique indicate that, at this concentration, the presence of the nanoparticles reduces the value of the thermal parameters of pure carrier liquids and both thermal diffusivity and effusivity decrease with increasing nanoparticles size, independently on the carrier liquid. The influence of the nanoparticles size is more pronounced for the thermal effusivity (relative change 24 %) compared with thermal diffusivity (relative change 7 %).

Keywords Magnetic nanofluids · Photopyroelectric technique · Thermal parameters · Type and size of nanoparticles

✉ C. Tripon
carmen.tripon@itim-cj.ro

1 National R&D Institute for Isotopic and Molecular Technologies, Cluj-Napoca, Romania

🍷 Springer

1 Introduction

Determination of thermal properties of magnetic nanofluids is important for many applications. The industrial applications of magnetic nanofluids as efficient cooling systems attracted high interest. A heat transfer enhancement could be obtained in devices and equipments where the heat transfer medium is a magnetic nanofluid. Furthermore, magnetic nanofluids have potential biomedical applications such as hyperthermia treatment and disease diagnosis for which thermal properties are important. The magnetic properties of magnetic nanofluids are the subject of various studies. On the other hand, data about their thermal properties are rarely found in the literature. Normally, the thermal properties of the magnetic nanofluids depend on the composition of the nanofluid: type size and concentration of nanoparticles, type of surfactant and carrier fluid. Even more, the values of the thermal parameters and their temperature behavior are correlated with structural changes and with the dynamics of the processes (drug delivery, for example) occurring inside the nanofluid.

In recent years, the photopyroelectric (PPE) technique proved to be very suitable when characterizing liquid samples. This is due to the fact that the thermal contact between a solid and a liquid (sensor/sample) is perfect and consequently, accurate results are obtained [1–5]. One of the recent applications of the PPE calorimetry is the thermal characterization of the magnetic nanofluids [6,7]. As it is well known, through the PPE calorimetry, one can obtain all static and dynamic thermal parameters of a liquid, by directly measuring two parameters, usually the thermal diffusivity and thermal effusivity [1–4]. The PPE technique, in various detection configurations, has been already used in order to find the influence of the carrier liquid, type of surfactant and concentration of nanoparticles, on the thermal parameters of the nanofluid [6,7].

In this paper we will investigate the influence of type and size of nanoparticles on the thermal parameters of some magnetic nanofluids. Two types of carrier liquids (transformer oil and polypropylene glycol) have been combined with two types of magnetic nanoparticles (Fe_3O_4 and $MnFe_2O_4$). The resulting magnetic nanofluids were investigated by using the two well-known PPE detection configurations: (1) the back (BPPE) detection combined with the thermal-wave-resonator-cavity (TWRC) scanning procedure was used for thermal diffusivity measurements; (2) the front (FPPE) configuration together with the frequency scanning technique was used for thermal effusivity investigations. In both detection configurations, the information was contained in the phase of the PPE signal.

2 Theoretical Aspects

The theory of the two PPE configurations "back" (BPPE) and "front" (FPPE), including the approximations for each particular case, together with schematic diagrams of the detection cells, has been largely described elsewhere [1,2,6]. The PPE signal is a complex one defined by an amplitude and a phase, both depending on the thermal parameters of the layers of the detection cell. We will give here only the resulting equations for the PPE signal.

2.1 Back Configuration

For a detection cell composed by three layers (transparent window, magnetic liquid "m", and pyroelectric sensor "p") in the particular detection case when the rear side of the window is opaque (the whole radiation is absorbed at this surface) and the sample and sensor are thermally thick (the thermal diffusion length in the layer is smaller than the geometrical thickness), the phase, θ, of the BPPE signal is given by [8]:

$$\Theta = \Theta_0 - L_m \left(\frac{\omega}{2\alpha_m} \right)^{1/2} \tag{1}$$

where θ_0 is a frequency independent phase offset, $\omega = 2\pi f$, with f = chopping frequency of radiation, L_m and α_m represent sample's (magnetic nanofluid in our case) thickness and thermal diffusivity, respectively.

The thermal diffusivity can be obtained by using the slope of the curves $\Theta = \Theta(f^{1/2})$ or $\Theta = \Theta(L_m)$. For this study we selected the second alternative: it is based on sample's thickness scan of the phase (TWRC scanning procedure) of the BPPE signal (at constant chopping frequency) [7,8]. The advantage of the method consists in the fact that the data processing does not request the exact knowledge of the sample's thickness, but only the sample's thickness variation. This method is a direct one and involves no calibration [9–12].

2.2 Front Configuration

As demonstrated before [13], in the case of a detection cell composed by two layers, directly irradiated opaque pyroelectric sensor "p" and thermally thick magnetic nanofluid "m," the equation of the normalized phase (normalization performed with empty sensor) of the FPPE signal is given by:

$$\Theta = \arctan \frac{(1 + R_{mp}) \sin(a_p L_p) e^{-a_p L_p}}{1 - (1 + R_{mp}) \cos(a_p L_p) e^{-a_p L_p}} \tag{2}$$

with:

$$(a_p)^{-1} = \mu_p = (2\alpha_p/\omega)^{1/2} \text{ and } R_{mp} = (b_{mp} - 1)/(b_{mp} + 1) \tag{3}$$

From Eq. 2 we can calculate R_{mp} as:

$$R_{mp} = \frac{\tan \Theta}{\left[\sin(a_p L_p) + \cos(a_p L_p) \tan \Theta \right] e^{-a_p L_p}} - 1 \tag{4}$$

and the sample's thermal effusivity as:

$$e_m = e_p \frac{1 + R_{mp}}{1 - R_{mp}} \tag{5}$$

In practice, one performs a frequency scan of the phase of the signal and finds the thermal effusivity by optimizing the fit performed on the experimental data with Eq. 2, with e_m as a fit parameter.

As a conclusion to this theoretical section, both thermal diffusivity and effusivity of a magnetic nanofluid can be measured by combining two configurations of the PPE technique: the back (BPPE) detection, combined with the thermal-wave-resonator-cavity (TWRC) scanning procedure (for thermal diffusivity) and the front (FPPE) configuration, together with the frequency scanning technique (for thermal effusivity).

3 Experimental

3.1 PPE Experimental Setup

The experimental setup for PPE calorimetry, in both front and back configurations, contains some typical components, and it was largely described in previous works [1,2,13]. In our experiments, the radiation source, a 100 mW YAG laser, was modulated from its power supply. The PPE signal is processed with a SR 830 lock-in amplifier.

Concerning the detection cells, in the BPPE configuration, the space between a directly irradiated opaque, thin (50 μm thick) and blackened metallic foil and a 540 μm thick LiTaO$_3$ sensor ($e_p = 3.6 \times 10^3$ Ws$^{1/2}$·m^{-2}·K^{-1} and $\alpha_p = 1.2 \times 10^{-6}$ m^2·s^{-1}), coated with gold electrodes on both faces, is filled with the magnetic nanofluid. In the FPPE configuration, the same LiTaO$_3$ sensor is situated in the front position (directly irradiated), and the magnetic nanofluid fills a glass cylinder (5 mm high) glued on the rear side of the sensor. In the BPPE configuration, the liquid's thickness variation is performed with a step of 0.03 μm (9062M-XYZ-PPP Gothic-Arch-Bearing Picomotor) and the data acquisition was taken at the end of each 50th step. The "rough" control of the liquid's thickness and the parallelism between window and sensor (BPPE), or backing and sensor (FPPE), are assured by 3- and 6-axis micrometric stages. During the scanning procedure, the liquid's thickness variation is very rigorously controlled, but its absolute thickness is not precisely known. Its correct value is obtained as a result of a fitting procedure [1,2,13]. The value of the chopping frequency in the BPPE configuration (1 Hz) was selected to fulfill the requests of the theoretical assumptions [14].

In the FPPE configuration, the frequency scan was performed in the 1 Hz–25 Hz range with a step of 0.5 Hz. It is important to point out that in this configuration the curve "normalized phase versus chopping frequency" is an oscillating function that intersects the frequency axis at some frequencies allowing the direct calculation of the sensors thermal diffusivity. In other words, the frequencies for which the normalized phase is zero are independent on the backing material; this is an important check for the validity of the measurement [2,13].

All the measurements were performed at room temperature. A computer with adequate software is used for data acquisition.

3.2 Experimental Synthesis of Nanofluids

Hydrophobic monodispersed iron oxide (Fe$_3$O$_4$) and manganese ferrite (MnFe$_2$O$_4$) nanoparticles were synthesized by high-temperature organic solution phase method
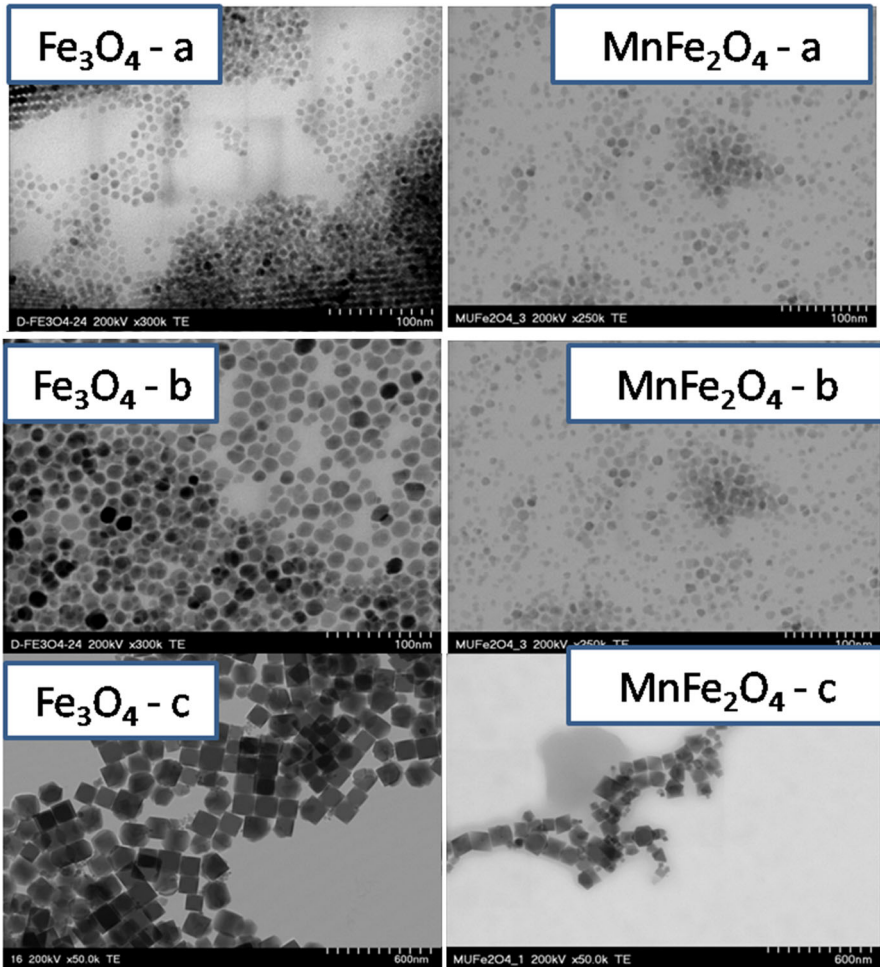
Fig. 1 Transmission electron microscopy (TEM) images of the as-synthesis nanopaticles (see Table 1)

[15]. The reaction of metal precursors, iron acetylacetonate $Fe(acac)_3$ and mangan acetylacetonate $Mn(acac)_2$ with hydrophobic stabilizer like oleic acid and oleylamine in a high boiling point solvent, benzyl ether, could lead monodispersed magnetic nanoparticles with controlled size and shape. The size of the particles is tuned by varying the concentration of the metal precursors, while the shape is controlled by the amount of the stabilizer added to reaction mixture (Fig. 1).

In a typical synthesis procedure, 2.28 g (6.4 mmol) of iron (III) acetylacetonate and 1.62 g (6.4 mmol) mangan (II) acetyl acetonate were mixed with 5 ml (4.45 g) oleic acid and different quantities of oleylamine in 40 ml dibenzylether. The iron (III) acetylacetonate or mangan (II) acetyl acetonate to oleic acid molar ratio was 1:2.5, while the molar ratio of oleic acid to oleylamine was adjusted in order to obtain different size and shape magnetic nanoparticles. All reaction conditions are summarized in

Table 1 Summary of reaction conditions

Sample	Fe (acac)$_3$/Mn(acac)$_2$:oleic acid (molar ratio)	Oleic acid:oleylamine (molar ratio)	Size (nm)	Shape
Fe$_3$O$_4$-a	1:2.5	1:2	10	Spherical
Fe$_3$O$_4$-b	1:2.5	2:1	20	Octahedral
Fe$_3$O$_4$-c	1:2.5	1:0	50	Cubic
MnFe$_2$O$_4$-a	1:2.5	1:2	10	Spherical
MnFe$_2$O$_4$-b	1:2.5	2:1	35	Octahedral
MnFe$_2$O$_4$-c	1:2.5	1:0	80	Cubic

The (mean) size of the nanoparticles in table was estimated by averaging at least 50 nanoparticles (TEM)
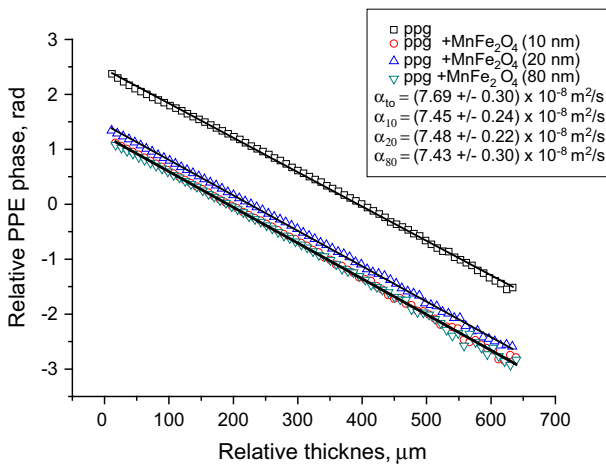

Fig. 2 The relative phase of the BPPE signal as a function of nanofluids' thickness for the magnetic nanofluids containing ppg as carrier liquid and MnFe$_2$O$_4$ as magnetic nanoparticles of different sizes (10 nm, 20 nm and 80 nm). $f = 1$ Hz

Table 1. First the solution was heated to 200 °C under argon atmosphere and vigorous stirring. After 1 h, the solution was heated to reflux and keep at this temperature for 1 h. Finally, the solution was cooled down, washed several times with a mixture of ethanol and hexane, separated magnetically and re-dispersed in toluene or other carrier solvent.

3.2.1 Phase Transfer

5 ml of toluene dispersed iron oxide or manganese ferrite magnetic nanoparticles were precipitated with 10 ml of ethanol. After sonication of 10 min, the solution was magnetically separated, washed three times with acetone and re-dispersed in carrier solution, like transformer oil or poly (propylene glycol) 2000.
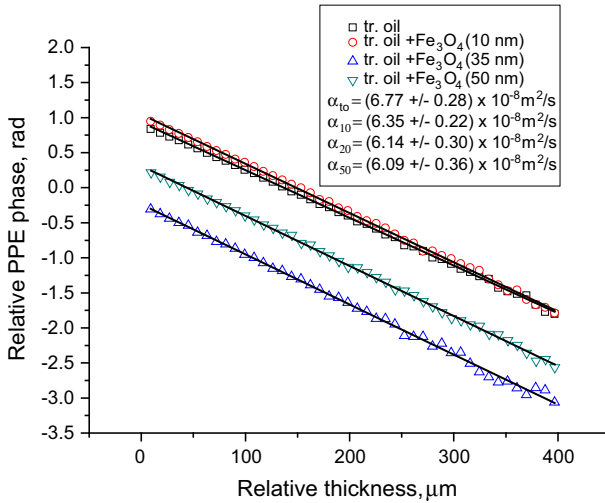
Fig. 3 The relative phase of the BPPE signal as a function of nanofluids' thickness for the magnetic nanofluids containing tr. oil as carrier liquid and Fe_3O_4 as magnetic nanoparticles of different sizes (10 nm, 35 nm and 50 nm). $f = 1\,Hz$
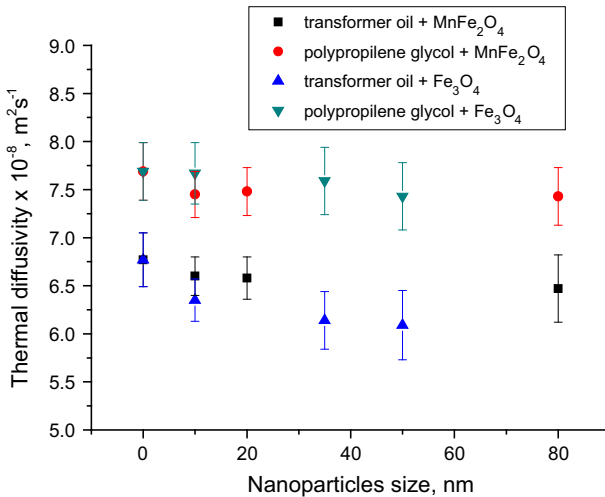

Fig. 4 The results obtained for the thermal diffusivity of the investigated magnetic nanofluids as a function of the nanoparticles' size

4 Results

4.1 Thermal Diffusivity

Figures 2 and 3 present typical nanofluids' thickness scans of the relative phase of the BPPE signal for the magnetic nanofluids containing polypropylene glycol (ppg) as carrier liquid and $MnFe_2O_4$ as magnetic nanoparticles, and transformer oil (tr. oil)
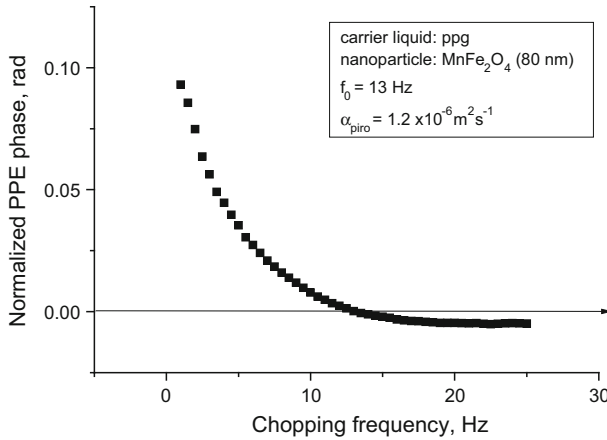
Fig. 5 Typical behavior of the normalized phase of the FPPE signal versus the chopping frequency for a magnetic nanofluid based on ppg as carrier fluid and with $MnFe_2O_4$ as magnetic nanoparticles (size 80 nm)
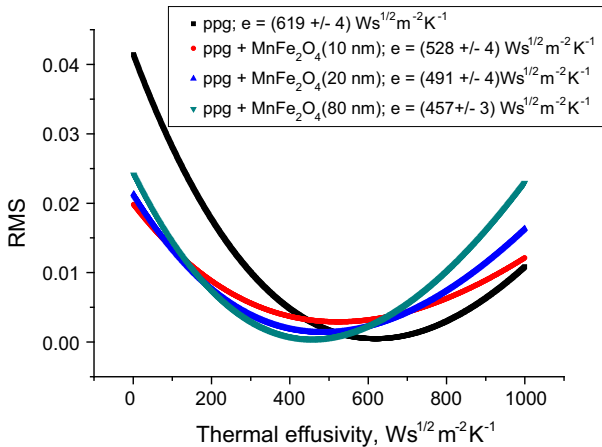

Fig. 6 Best fits obtained with Eq. 2 on the experimental data for the magnetic nanofluids containing ppg as carrier liquid and $MnFe_2O_4$ as magnetic nanoparticles. Nanoparticles size 10 nm, 20 nm and 80 nm. The minimum of the curves indicates the value of the thermal effusivity, associated with the best fit

as carrier liquid and Fe_3O_4 as magnetic nanoparticles, respectively. The size of the nanoparticles is the parameter. Results for pure carrier liquids have been also inserted in figures for comparison. The value of the thermal diffusivity was calculated from the slope of the curve, accordingly to Eq. 1.

The results obtained for the values of the thermal diffusivity for all the combinations polypropylene glycol/ transformer oil and $MnFe_2O_4/Fe_3O_4$ are displayed in Fig. 4.

4.2 Thermal Effusivity

Figure 5 displays a typical behavior of the normalized phase of the FPPE signal as a function of the chopping frequency of the incident radiation for a magnetic nanofluid
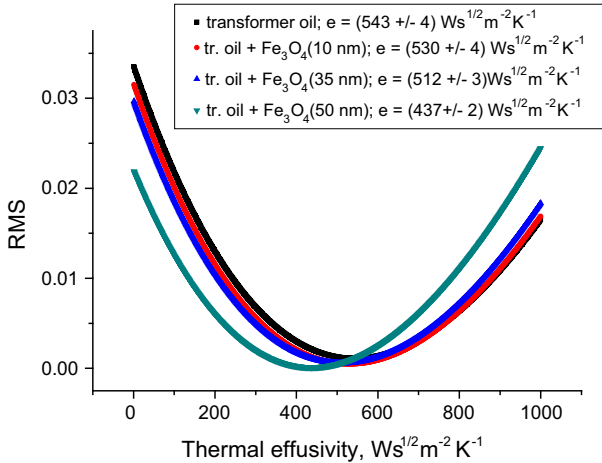
Fig. 7 Best fits obtained with Eq. 2 on the experimental data for the magnetic nanofluids containing tr. oil as carrier liquid and Fe_3O_4 as magnetic nanoparticles. Nanoparticles size 10 nm, 35 nm and 50 nm. The minimum of the curves indicates the value of the thermal effusivity, associated with the best fit
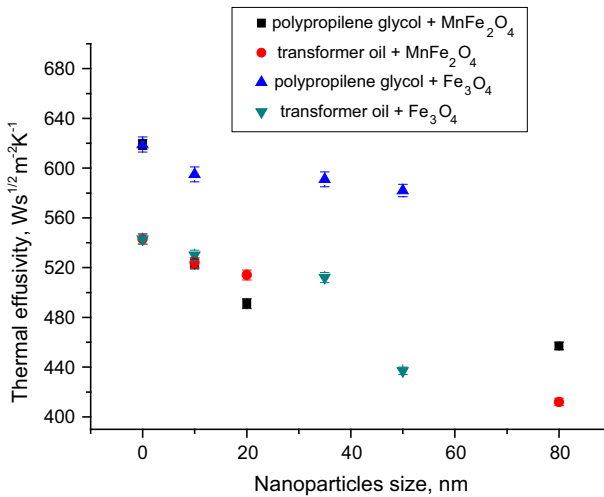

Fig. 8 The results obtained for the thermal effusivity of the investigated magnetic nanofluids as a function of the nanoparticles' size

based on ppg as carrier fluid and with $MnFe_2O_4$ as magnetic nanoparticles (size 80 nm). The critical frequency "f_0" is 13 Hz, leading, as standing in the theoretical section, to the correct value for the sensor's thermal diffusivity ($\alpha_{pyro} = 1.2 \times 10^{-6}\, m^2 \cdot s^{-1}$) [16].

Figures 6 and 7 present the best fits obtained with Eq. 2 on the experimental data for the magnetic nanofluids containing polypropylene glycol (ppg) as carrier liquid and $MnFe_2O_4$ as magnetic nanoparticles, and transformer oil (tr. oil) as carrier liquid and Fe_3O_4 as magnetic nanoparticles, respectively. The parameter is also the size of the nanoparticles. Results for pure carrier liquids have been also inserted in figures for

Table 2 Room temperature values of thermal diffusivity and effusivity for the combinations polypropylene glycol/transformer oil and $MnFe_2O_4/Fe_3O_4$ as obtained from PPE investigations

Magnetic nanofluid	Thermal diffusivity $\times 10^{-8} (m^2 \cdot s^{-1})$	Thermal effusivity $(Ws^{1/2} \cdot m^{-2} \cdot K^{-1})$
ppg	7.69 ± 0.30	619 ± 4
tr. oil	6.77 ± 0.28	543 ± 4
ppg + $MnFe_2O_4$		
Size: 10 nm	7.45 ± 0.24	528 ± 4
Size: 20 nm	7.48 ± 0.22	491 ± 4
Size: 80 nm	7.43 ± 0.30	457 ± 3
ppg + Fe_3O_4		
Size: 10 nm	7.67 ± 0.31	595 ± 4
Size: 35 nm	7.59 ± 0.26	591 ± 4
Size: 50 nm	7.43 ± 0.30	582 ± 4
tr. oil + $MnFe_2O_4$		
Size: 10 nm	6.60 ± 0.20	524 ± 4
Size: 20 nm	6.58 ± 0.22	514 ± 4
Size: 80 nm	6.47 ± 0.35	412 ± 4
tr. oil + Fe_3O_4		
Size: 10 nm	6.35 ± 0.22	530 ± 4
Size: 35 nm	6.14 ± 0.30	512 ± 3
Size: 50 nm	6.09 ± 0.36	437 ± 2

The uncertainties for both thermal diffusivity and effusivity are calculated only as a result of the standard deviation of the fitting procedures

comparison. The minimum of the curves in Figs. 6 and 7 is associated with the value of the thermal effusivity.

The results obtained for the values of the thermal effusivity for all the combinations polypropylene glycol/ transformer oil and $MnFe_2O_4/Fe_3O_4$ are displayed in Fig. 8.

A synthesis of the results obtained for the two measured thermal parameters, thermal diffusivity and effusivity for all the combinations polypropylene glycol/transformer oil and $MnFe_2O_4/Fe_3O_4$, is presented in Table 2. The remaining thermal parameters, the thermal conductivity k and volume specific heat, C can be derived by using well-known relationships: $k = C\alpha$ and $C = e/sqrt(\alpha)$.

5 Discussions and Conclusions

5.1 Morphology of the Nanofluids

Figure 1 shows transmission electron microscopy (TEM) images of the as-synthesized iron oxide and manganese ferrite for different samples prepared in different reaction conditions. For the ratio 1:2 oleic acid oleylamine, spherical nanoparticles of about 10 nm size were obtained (see Fig. 1: Fe_3O_4-a, $MnFe_2O_4$-a). For intermediary molar ratio of 2:1, quasi-regular octahedral shape nanoparticles were obtained of 20 nm to

30 nm (see Fig. 1: Fe_3O_4-b, $MnFe_2O_4$-b). When just oleic acid is used for stabilizing the magnetic nanoparticles larger cubic nanoparticles of 60 nm to 80 nm were obtained (see Fig. 1: Fe_3O_4-c, $MnFe_2O_4$-c). So, it is noticed that the size of the nanoparticles increases with the decreasing of the relative concentration of oleylamine. It should also be pointed out that the particles larger than 10 nm showed gradually octahedral and finally cubic shape when they are synthesized in a reaction mixture containing smaller concentration of oleylamine (octahedral shape) and no oleylamine, the cubic shape. This demonstrates the strong effect of the oleic acid/oleylamine molar ratio on the nanocrystals growth rate due to the different binding ability of the two stabilizers onto crystal facets.

5.2 Thermal Parameters

Concerning the PPE investigations, the detection configurations are already largely used, so the main result of this paper consists in the values included in Table 2. As a general conclusion, the presence of the nanoparticles, for this concentration range, decreases the value of the thermal parameters of pure carrier liquids and both thermal diffusivity and effusivity decrease with increasing nanoparticles size, independently on the carrier liquid. As an order of magnitude, the influence of the nanoparticles size is more pronounced for the thermal effusivity (maximum relative change 24 %) compared with thermal diffusivity (maximum relative change 7 %).

We have to point out that this decrease of the values of dynamic thermal parameters of the nanofluids due to the presence of the nanoparticles is valid only at these lower concentrations (about $50\,mg \cdot ml^{-1}$mg·ml). At much higher concentrations of nanoparticles ($150\,mg \cdot ml^{-1}$–$350\,mg \cdot ml^{-1}$) the values of the thermal parameters of the nanofluids increase compared with the pure carrier liquid and increase with increasing nanoparticles concentrations [6,7]. At higher nanoparticles concentration, the explanation is clear due to the values of the nanoparticles' thermal parameters which are higher than those of the carrier liquids. The results obtained in this paper for low nanoparticles' concentration seem at a first view controversial. However, it is well known that in the case of binary liquid mixtures (especially when the liquids are associative) or liquid/solid mixtures (when the solid component forms chain structures) the behavior of the thermal parameters with the composition is usually nonlinear (presenting a minimum at a given concentration, or a percolation threshold due to the fact that the additivity rule is not respected) [1,3,17]. This seems to be the case of the investigated nanofluids: at low nanoparticles' concentration, the value of the nanoparticle's thermal parameter is not important yet (has no contribution to the value of the nanofluid's total thermal parameter), but the structures presented in Fig. 1 disturb the thermal conduction in the fluid. For higher nanoparticles concentrations, the values of the thermal parameters of the nanoparticles themselves start to influence the thermal conduction and the values of the thermal parameters of the nanofluid increase with increasing nanoparticles concentration [7].

References

1. D. Dadarlat, Laser Phys. **19**, 1330 (2009)
2. D. Dadarlat, C. Neamtu, in *Thermal Wave Physics and Related Photothermal Techniques: Basic Principles and Recent Developments*, ed. By E.M. Marin (Transworld Research Network, Trivandrum, Kerala, 2009)
3. A. Sikorska, D. Dadarlat, B.B.J. Linde, M. Streza, C. Neamtu, A. Sliwinski, J. Phys. IV **137**, 341 (2006)
4. D. Dadarlat, J. Therm. Anal. Calorim. **110**, 27 (2012)
5. D. Dadarlat, M. Streza, M.N. Pop, V. Tosa, S. Delenclos, S. Longuemart, A.H. Sahraoui, J. Therm. Anal. Calorim. **101**, 397 (2010)
6. D. Dadarlat, S. Longuemart, R. Turcu, M. Streza, L. Vekas, A.H. Sahraoui, Int. J. Thermophys. **35**, 2032 (2014)
7. D. Dadarlat, P.R.N. Misse, A. Maignan, E. Guilmeau, R. Turcu, L. Vekas, C. Tudoran, M. Depriester, A.H. Sahraoui, Int. J. Thermophys. **36**, 2441 (2015)
8. M. Marinelli, F. Mercuri, U. Zammit, R. Pizzoferrato, F. Scudieri, D. Dadarlat, Phys. Rev. B **49**, 9523 (1994)
9. J. Shen, A. Mandelis, Rev. Sci. Instrum. **66**, 4999 (1995)
10. J. Shen, A. Mandelis, H. Tsai, Rev. Sci. Instrum. **69**, 197 (1998)
11. J.A. Balderas-Lopez, A. Mandelis, J.A. Garcia, Rev. Sci. Instrum. **71**, 2933 (2000)
12. J.A. Balderas-Lopez, A. Mandelis, Rev. Sci. Instrum. **74**, 700 (2003)
13. D. Dadarlat, C. Neamtu, Meas. Sci. Technol. **17**, 3250 (2006)
14. M. Chirtoc, J.S. Antoniov, M. Egee, in *Proceeding of 10-th International Conference on Photoacoustic and Photothermal Phenomena*. (Rome, 1998), pp. 84–86
15. S. Sun, H. Zeng, D.B. Robinson, S. Raoux, P.M. Rice, S.X. Wang, G. Li, J. Am. Chem. Soc. **126**, 273 (2004)
16. M. Nakamura, S. Takekawa, K. Kitamura, Opt. Mater. **32**, 1410 (2010)
17. C. Neamtu, D. Dadarlat, M. Chirtoc, A.H. Sahraoui, S. Longuemart, D. Bicanic, Instrum. Sci. Technol. **34**, 225 (2006)